# Paleoceanography and Paleoclimatology

## RESEARCH ARTICLE

**Key Points:**
- Coral Sr/Ca-sea-surface temperature variations from the northern South China Sea are a reliable proxy of El Niño–Southern Oscillation variability
- Intensified El Niño–Southern Oscillation variability occurred during the late Medieval Climate Anomaly
- Unforced internal variability within the climate system likely play a prominent role in modulating El Niño–Southern Oscillation variability

# ENSO Variability During the Medieval Climate Anomaly as Recorded by *Porites* Corals From the Northern South China Sea

**Leilei Jiang[1], Kefu Yu[1,2] , Shichen Tao[1] , Shaopeng Wang[1], Tao Han[1], and Wei Jiang[1]**

[1]Guangxi Laboratory on the Study of Coral Reefs in the South China Sea, Coral Reef Research Centre of China, School of Marine Sciences, Guangxi University, Nanning, China, [2]Southern Marine Sciences and Engineering Guangdong Laboratory (Zhuhai), Zhuhai, China

**Abstract** The El Niño–Southern Oscillation (ENSO) dominates interannual climate variability worldwide and has important environmental and socio-economic consequences. However, determining the evolution of ENSO variability and its long-term response to climate forcing remains an ongoing challenge owing to the limited instrumental records. In this study, we quantified ENSO variability via an empirically calibrated threshold and sliding variance windows using monthly sea-surface temperature (SST) anomalies based on *Porites* coral Sr/Ca records from the Xisha Islands in the northern South China Sea. Instrumental SST anomalies from the Xisha Islands correctly captured increasing ENSO variability in the twentieth century, with ENSO detection skills similar to those for Niño3.4 regions. Coral Sr/Ca-SST anomalies can also serve as sensitive and robust proxies for ENSO variability. Sub-fossil coral Sr/Ca-SST anomalies indicated intensified ENSO variability at the end of the Medieval Climate Anomaly (MCA) from 1149 to 1205 ± 4.9 (2$\sigma$) Common Era (CE). Combining our records with other ENSO-sensitive proxy reconstructions from the tropical Pacific, we observed fluctuating ENSO variability during the MCA and intensified ENSO variability for the late MCA. Considering the fewer and low intensity fluctuations associated with external climate forcing and the absence of a coherent temporal correspondence of ENSO activity with solar irradiance and volcanic eruption during the MCA, we hypothesized that the internal dynamics of the climate system play a prominent role in modulating ENSO variability and its evolution, which is supported by unforced climate model simulations and coral reconstructions across the tropical Pacific.

## 1. Introduction

The El Niño–Southern Oscillation (ENSO) is an inherently unstable climatic oscillation of the tropical Pacific oceanic–atmospheric system between positive (El Niño) and negative (La Niña) phases with a periodicity of 2 to 8 years (Timmermann et al., 2018; Wang & Fiedler, 2006). The impacts of ENSO activity can be transmitted worldwide through atmospheric teleconnections, significantly altering global redistribution of heat and moisture fluxes (Alexander et al., 2002; Diaz & Markgraf, 2000; Trenberth, 1997). Therefore, ENSO has dramatic impacts on agriculture, weather, ecological environment, society, and economy (Cai et al., 2014; Sarachik & Cane, 2010). Although instrumental observations can be used to test the predictive skills of climate models on interannual timescales, these short records limit the improvement of models that simulate ENSO variability. ENSO reconstructions from paleoclimate archives, which extend the time span of instrumental records, can provide valuable perspectives on ENSO variability, climate forcing, and model investigations (Schmidt, 2010). Furthermore, determining the range of natural ENSO variability over the last millennium is essential for understanding the underlying mechanisms of ENSO and for predicting future ENSO activity under anthropogenic climate change.

The Medieval Climate Anomaly (MCA) is generally defined as occurring from approximately 950 to 1,250 Common Era (CE) and this time interval was subjected to mostly warm conditions in Northern Hemisphere temperature reconstructions (Masson-Delmotte et al., 2013). Although numerous studies have provided some clarifications on ENSO activity during the MCA, paleo-ENSO variability and the response to climate forcing during this period remains poorly understood and vigorously contested (Emile-Geay et al., 2013b; Sadekov et al., 2013). According to some regional evidence, the medieval period was characterized by
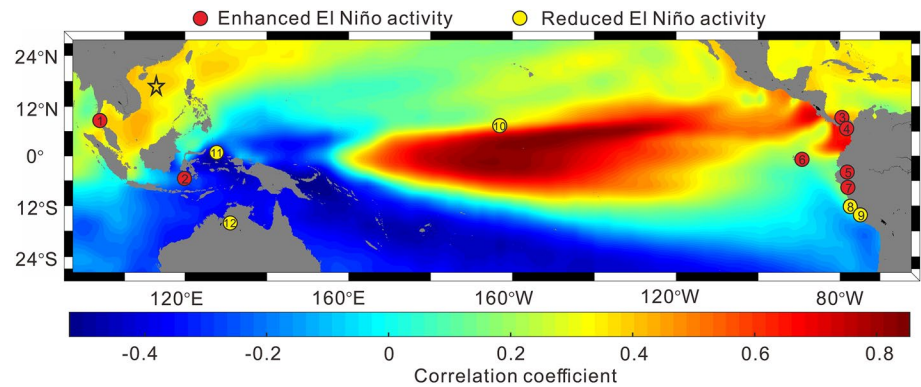
**Figure 1.** Spatial correlation between monthly sea-surface temperature (SST) of the tropical Pacific and Niño3.4 SST during 1,982–2016 CE (with tropical Pacific SST lags by 6 months). The source of SST data is Optimum Interpolation Sea Surface Temperature version 2 data product (NOAA OI SST v2; Reynolds et al., 2002). A significant positive correlation in the South China Sea (SCS) ($r = 0.42$, $n_{eff} = 22$, $p_{adj} = 0.02$ at the Xisha Islands) indicates warmer (colder) conditions in the SCS during El Niño (La Niña). Red dots with numbers indicate enhanced El Niño activity during the MCA, whereas yellow dots with numbers indicate reduced El Niño activity. Further information about these data used for each location can be found in Table S3 of Supporting Information. Star indicates the location of the sampling sites in the Xisha Islands. CE, Common Era; MCA, Medieval Climate Anomaly; SCS, South China Sea; SST, sea-surface temperature.

persistently weak ENSO variability (Cobb et al., 2013; Rein et al., 2005), whereas a number of proxy records have demonstrated strong ENSO variability during this time interval (Ledru et al., 2013; Moy et al., 2002; Rustic et al., 2015; Tan et al., 2019; Toth et al., 2015). The sensitivity of ENSO to external climate forcing also remains a subject of considerable debate (Dee et al., 2020). Studies on the ocean dynamical thermostat mechanism have revealed that positive tropical radiative forcing counteracts the development of El Niño events (Booth et al., 2006; Clement et al., 1996; Goodwin et al., 2014; Salvatteci et al., 2013). Nevertheless, several studies have found no obvious relationship between irradiance or volcanism and ENSO activity. Instead, they suggest that the majority of ENSO variability is modulated by internal variability of ENSO system (Cobb et al., 2003, 2013; Graham et al., 2011). In addition, climate model simulations have demonstrated that stochastic modulation of the climate system leads to the changes in ENSO variability (Wittenberg, 2009). These results indicate complex and contradictory ENSO behavior during the MCA and emphasize the necessity of expanding high-resolution ENSO reconstructions.

Fast-growing massive hermatypic corals (growth rate of up to 2 cm/year) contain an array of geochemical tracers within their skeletons (Yu, 2012). Therefore, coral records can provide high-fidelity archives for continuous, monthly to annually resolved paleoclimatic and paleoceanographic studies (Cobb et al., 2003; Corrège et al., 2000; McGregor et al., 2013; Tierney et al., 2015; Tudhope et al., 2001). The analysis of oxygen isotopes ($\delta^{18}O$) in coral skeletons has been a primary source of information on seasonal and interannual variability (Cole et al., 1993; Yu et al., 2005). However, coral $\delta^{18}O$ is a function of both the sea-surface temperature (SST) and $\delta^{18}O$ composition of the ambient seawater ($\delta^{18}O_{sw}$). Thus, it is normally difficult to extract SST from the overall isotope signals. To circumvent this ambiguity, Smith et al. (1979) found the inverse relationship between SST and strontium to calcium (Sr/Ca) ratios of corals and proposed the equations. After that, Beck et al. (1992) suggested to measure coral Sr/Ca ratios via the high-precision Thermal Ionization Mass Spectrometry to reconstruct SST with monthly resolution. Subsequently, the variations in coral Sr/Ca have become an established tracer for SST variability on seasonal and interannual timescales (Corrège et al., 2000; Gagan et al., 1998). Therefore, coral skeletons Sr/Ca has been widely served for paleo-ENSO reconstructions in tropical and subtropical oceans (Alibert & McCulloch, 1997; DeLong et al., 2013; McCulloch et al., 1994).

The South China Sea (SCS) contains widely distributed corals and is sensitive to ENSO variability (Han et al., 2020; Yu, 2012; Figure 1). Coral Sr/Ca-SST reconstructions from the SCS have been systematically developed in recent decades, yielding a series of published coral Sr/Ca data that provide a high-resolution Holocene climate history and ENSO records (Mitsuguchi et al., 2008; Yu et al., 2004, 2005). However, most studies have only concentrated on ENSO periodicity and have rarely involved the MCA, especially for the
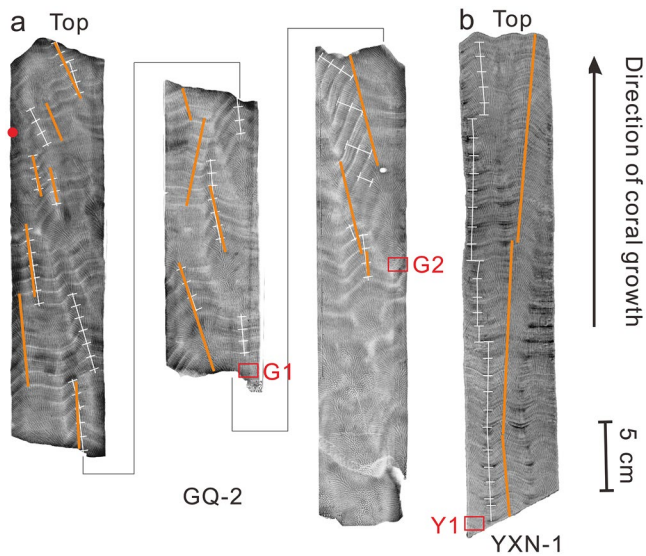
**Figure 2.** X-radiograph positive images of (a) sub-fossil (GQ-2) and (b) modern (YXN-1) *Porites lutea* coral core slabs. White and orange lines indicate the annual density banding and the sub-sampling transects along the major growth axis, respectively. Red rectangles indicate the location of thin sections that were used to assess the preservation of coral aragonite. Red point denotes the location of sample selected for U-Th dating.

evolutionary characteristics of ENSO variability and the corresponding climate forcing (Sun et al., 2005; Wei et al., 2007). Here, we used instrumental and reanalysis data sets of SST from the Xisha Islands, which is an archipelago in the northern SCS, to analyze the impact of ENSO (Niño3.4) in this region. Subsequently, we investigated ENSO variability based on monthly sub-fossil coral Sr/Ca-SST from 1149 to 1205 ± 4.9 (2σ) CE, which is a period coinciding with the late MCA. Our aim is to identify the characteristics of ENSO variations that occurred during the MCA and to analyze the possible forcing factors.

## 2. Climatic Setting of Study Area

The SCS, a semi-enclosed marginal sea in the northwestern region of the tropical Pacific (Figure 1), is an important area for the transport of moisture and energy between low and middle-high latitudes (Su et al., 2010). The Xisha Islands (15°–17°N, 111°–113°E) are located at the northwestern SCS (Figure S1). Satellite-derived SST (NOAA OI SST v2; Reynolds et al., 2002) from the Xisha Islands demonstrate a mean SST of 27.3 ± 0.4 (1σ)°C and exhibit annual cycles (Figure S2), with a mean maximum of 29.2 ± 0.4 (1σ)°C in the summer (June–July–August: JJA) and a mean minimum of 24.7 ± 0.6 (1σ)°C in the winter (December–January–February: DJF) from 1982 to 2016 CE (Figure S1). Observational results have revealed that ENSO activity remotely affects the SST in the SCS (Figure 1), suggesting that warmer (colder) conditions persist during El Niño (La Niña) events. Mature ENSO phases that usually occur in boreal winter remotely affect the climate of the SCS via the so-called "atmospheric-bridge" of atmospheric circulation changes (Klein et al., 1999). When El Niño events occur, the anomalous anticyclone over the western Pacific weakens monsoons, which would reduce cloudiness, increase solar radiation, and cause the positive SST anomalies (SSTA) in the northern SCS (Han et al., 2020; Wang et al., 2000; Yan et al., 2010). Meanwhile, the weakened East Asia Trough decreases the sea-level pressure in Aleutians Island, which would increase the land surface temperature, strengthen southern winds, and yield a decreased winter monsoon and increased SST in the SCS (Guo & Wang, 1990; Song et al., 2012; Zhu & Xie, 1988). For example, the anomalous warm events in the SCS from 1997 to 1998 CE were closely related to the strong El Niño event during that period (Wang et al., 2004, 2006). The reverse phenomena take place during La Niña events.

## 3. Materials and Methods

### 3.1. Coral Samples

Two coral cores from the Xisha Islands were obtained from *Porites lutea* colonies using an underwater hydraulic drill in late June 2008 CE. The first sample GQ-2, which was collected from an in situ sub-fossil coral, was recovered from ∼5 m water depth on the fringing reef of Ganquan Island (16°30′28″N, 111°35′10″E; Figure S3). The second sample YXN-1 was collected from a living coral at ∼6 m water depth off Yongxing Island (16°50′27″N, 112°19′34″E), approximately 80 km from Ganquan Island (Figure S3). YXN-1 was used to calibrate the coral Sr/Ca-SST relationship in the Xisha Islands.

The obtained coral samples were cut into ∼7 mm thick slices along their major growth directions using a circular diamond saw. These slices were soaked in 5% $H_2O_2$ for 48 h, cleaned three times in an ultrasonic bath using deionized water, and air-dried in a 60°C oven for 48 h. After removing all the organic matter and surface contaminants, the coral slices were X-ray photographed to identify the annual-density banding patterns and determine the microsampling paths. According to the X-radiograph images (Figure 2), the mean extension rate of GQ-2 was 9 mm/year, ranging from 8 to 10 mm/year. The mean extension rate of YXN-1 was 12 mm/year, ranging from 10 to 12 mm/year (Table S1).

Three blocks extracted from the middle and bottom of the sub-fossil coral sample and the bottom of the modern coral sample were investigated for possible skeletal diagenetic alteration (Figure 2). First, a part of

the blocks was used for X-ray diffraction (XRD) analyses (Rigaku Ultima IV) to quantify the calcite content. The sub-fossil coral contained <0.2% calcite content, which is similar to that of modern coral (Figure S4). Considering that inorganic aragonite crystals could not be detected by XRD analyses, scanning electron microscopy (SEM) analyses (Hitachi SU5000) were used to distinguish the presence of secondary aragonite needles. A comparison of the SEM images for the other part of the blocks showed an excellent preservation level with respect to the primary porosity for modern and sub-fossil corals, as well as the absence of secondary minerals and diagenetic alteration (Figure S5).

### 3.2. Microsampling and Sr/Ca Analyses

Slabs were micro-milled along the maximum growth axis of the corallite fan and the path perpendicular to the annual-density bands using a digitally controlled milling machine (Alibert & McCulloch, 1997; DeLong et al., 2013; Fairbanks & Dodge, 1979; Felis et al., 2000; Marshall & McCulloch, 2002; Figure 2). According to the average extension rate of each coral, we continuously extracted coral skeletal powder with monthly resolution by milling at 2-mm depth, 2-mm width, and 0.8–1-mm increments. To ensure that the sampling paths followed the optimum sampling paths and avoided the valleys (Delong et al., 2013), all the coral slices after microsampling were X-ray photographed again (Figure S6).

Analyses of coral Sr/Ca were conducted on a Varian Vista Pro (Varian Inc.) inductively coupled plasma atomic emission spectroscope at Guangxi University, following previously described techniques (Yu et al., 2005). Each powdered aragonite coral sample was weighed using a microbalance (sample weights ranged from 0.8 to 1.0 mg) and placed into micro centrifuge tubes. Subsequently, each coral sample was completely dissolved in 2% $HNO_3$, such that the mass of final solution (8–10 g) was 10,000 times that of the original sample. The $Ca^{2+}$ concentration was targeted to ~40 ppm and within the calibration range from 10 to 45 ppm. Strontium and Ca wavelengths were simultaneously detected in three coral sample replicates. All obtained coral Sr/Ca ratios were corrected for instrument drift using standard-sample bracketing methods described by Schrag (1999). The in-house *Porites* coral standard (NS-1) collected from the SCS was dissolved in 2% $HNO_3$ and analyzed after every two coral samples. Then, the raw coral Sr/Ca data were linearly corrected using this in-house standard. Furthermore, the international coral standard (JCp-1 *Porites* spp.) was treated in the same way and analyzed along with the coral samples (Okai et al., 2002). The mean Sr/Ca value for the JCp-1 standard obtained in this study was 8.647 ± 0.069 (2$\sigma$) mmol/mol ($n = 127$), which is within analytical uncertainty of the accepted mean for JCp-1 (8.838 ± 0.089 (2$\sigma$) mmol/mol; Hathorne et al., 2013). The analytical precision for the coral Sr/Ca data was 0.016 mmol/mol (1$\sigma$) obtained from the repeated measurement ($n = 529$) of the in-house reference standard solutions (NS-1). This yielded an uncertainty of ~0.3°C according to the coral Sr/Ca-SST relationship of 0.0497 mmol/mol per 1°C from the Xisha Islands (see Section 4.3).

### 3.3. Chronology Construction

Growth chronologies for each coral core were developed by the cross-validation of visually counting the annual-density bands from the X-radiograph images and the pronounced annual cycle of coral Sr/Ca records. The modern coral sample YXN-1, for which the outermost band represented ongoing growth as of June 2008 CE, has a 28-year continuous growth record for 1,980–2007 CE. The sub-fossil coral sample GQ-2 was uranium-thorium (U-Th) dated using a Nu Plasma high resolution multicollector inductively coupled plasma mass spectrometer at the Radiogenic Isotope Facility of the University of Queensland. Yu et al. (2006, 2012) have described the details of the sample preparation and analytical method. GQ-2 was dated at 1200.1 ± 4.9 (2$\sigma$) CE (Table S2). According to the pronounced annual cycles of the coral Sr/Ca records, the lifespan of GQ-2 was identified to be in the period from 1149 to 1205 ± 4.9 (2$\sigma$) CE, corresponding to the late MCA. Considering the pronounced annual cycle of SST from the Xisha Islands for the period of 1982–2016 CE (Figure S2), we assigned the maximum and minimum coral Sr/Ca value in each annual cycle to the coldest (January) and warmest (June) months, respectively. We converted the coral Sr/Ca values into monthly resolved time series (12 points per year) by constructing a linear interpolation between these tie points.

## 4. Data Analysis

### 4.1. Data Sources

Monthly SST used in this study were collected from the Met Office Hadley Center Sea Ice and Sea Surface Temperature (HadISSTv1.1) database, which provides monthly SST data from the year 1870 onward, with a spatial resolution of $1° \times 1°$ (Rayner et al., 2003). The SST records from the SCS and the Xisha Islands were set to the mean SST for the region of 2.5°–22.5°N, 100°–120°E and 16°–17°N, 111.5°E–112.5°E, respectively. Both include the coral sites of this study. A commonly used index for representing SST variability associated with ENSO is the Niño3.4 SST index (Trenberth, 1997), which serves as the target climate signal for paleo-ENSO reconstruction (e.g., Cobb et al., 2003; Emile-Geay et al., 2013a, 2013b). Our overarching objective with these data was to demonstrate that instrumental SST data from the northern SCS accurately detects historical ENSO events. Therefore, we selected Niño3.4 SST, the mean SST for the region of 5°S–5°N, 170°–120°W, as the arbiter of ENSO variability. Modern observed ENSO events were defined following the methodology of Oceanic Niño Index, which is the 3-month moving mean of the HadISSTv1.1 SSTA (Rayner et al., 2003) in the Niño3.4 region that exceeds ±0.5°C for five or more consecutive overlapping 3-month periods (Hereid, Quinn, & Okumura, 2013; Larkin & Harrison, 2005).

### 4.2. Data Processing

To explore the periodic variability within SST records, the multi-taper method (MTM) spectral analysis was applied to the detrended and normalized SST series using the k-Spectra software package v.1.17 (Spectra Works; Ghil et al., 2002; Figure S7). The number of tapers ($k$) and the bandwidth parameter ($p$) were set to three and two, respectively, which are suitable for climate records with a few hundred time points. To isolate the interannual variability, seasonal variations were removed to generate monthly SSTA calculated as deviations from the respective timescale climatology for each SST record. Then, a 13-month running mean was applied to the monthly SSTA. We applied different band-pass filter windows representative of ENSO periodicities (e.g., 2–7-year, 2–8-year, and 3–7-year) to the SSTA from the Xisha Islands and Niño3.4 regions for the period of 1960–2016, and this analysis suggests that the SST from the Xisha Islands displays high sensitivity to ENSO activity (Figure S8). We focused on the 3–7-year band-pass filter for our analysis to ensure minimal influence from interactions between ENSO and Asian monsoon variability (Mitsuguchi et al., 2008; Yan et al., 2015), as well as amplitude modulation of the quasi-biennial cycle in the SCS (Charles et al., 1997; Han et al., 2020; Hu et al., 2020; Yan et al., 2017). Sliding variance windows can assist in determining the overall strength of ENSO signal at a particular time and have historically been employed to investigate the changes in ENSO variability (Cobb et al., 2003; Li et al., 2011). Here, we calculated a 31-year sliding variance for the filtered SSTA to investigate the evolution of ENSO variability (D'Arrigo et al., 2005; Wilson et al., 2010). We considered the effective degrees of freedom ($n_{eff}$) when conducting the significance tests ($p_{adj}$) for correlation analysis (Box et al., 1976; Trenberth, 1984; see Supporting Information for additional details).

We analyzed the ENSO detection skill with respect of the SST from the Xisha Islands using empirically calibrated threshold method proposed by Hereid, Quinn, and Okumura (2013). Based on the positive correlation between the filtered SSTA from the Xisha Islands and Niño3.4 regions (Figure S8), we classified the positive and negative SST excursions from the Xisha Islands as potential El Niño and La Niña events, respectively. According to the peaks of the filtered SSTA, we set the initial El Niño (La Niña) event threshold to 0.01°C (−0.01°C) for the Xisha SSTA and increased (decreased) the threshold in steps of 0.01°C. We recorded the peaks that exceeded the set threshold and defined them as ENSO events. We independently optimized the El Niño and La Niña threshold levels for the Xisha SSTA to maximize the percentage of correctly identified ENSO events (ENSO detection skill) and minimize falsely identified (false positives) and missed (false negatives) ENSO events.

### 4.3. Coral Sr/Ca Thermometer

Modern coral Sr/Ca records were significantly correlated with instrumental SST from the Xisha Islands for the period of 1980–2007 CE (Figure 3a). We performed a reduced major axis (RMA) regression analysis to calibrate the coral Sr/Ca–SST relationship. This regression technique provides more reliable and accurate
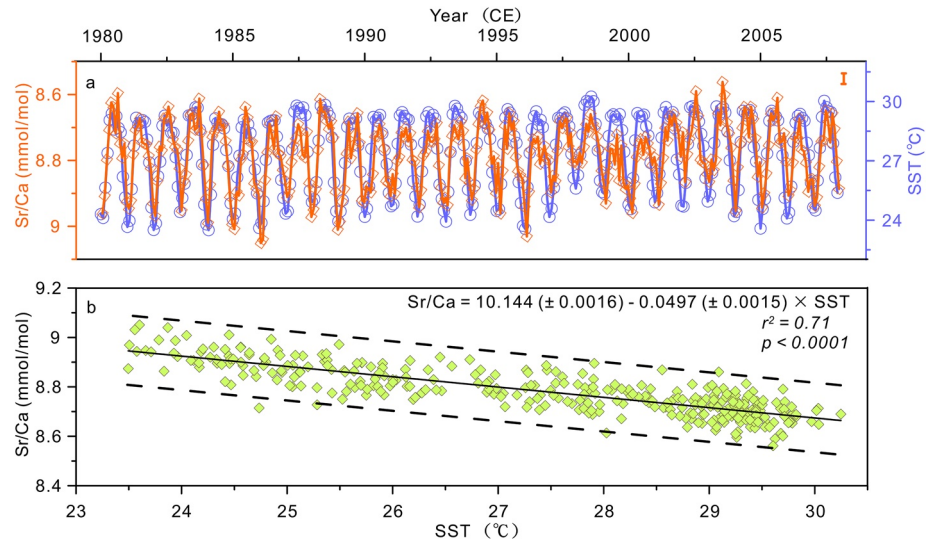
**Figure 3.** Calibration of the Sr/Ca thermometer in modern *Porites lutea* coral. (a) Comparisons of modern coral (YXN-1) Sr/Ca records (orange line) and instrumental SST (purple line; Rayner et al., 2003) from the Xisha Islands for 1980–2007 CE. Vertical error bar on the top-right indicates the analytical precision of 0.016 mmol/mol (1σ) in this study. (b) Regression of modern coral Sr/Ca records against instrumental SST for the period of 1980–2007 CE. The dashed lines indicate 95% confidence intervals. CE, Common Era; SST, sea-surface temperature.

estimates by minimizing the residuals in both the dependent variables and independent variables (Solow & Huppert, 2004). We used the RMA software (v.1.17) for the regression calculations (Bohonak, 2004). A corresponding linear regression equation can be proposed as follows (Figure 3b):

$$Sr/Ca\,(mmol/mol) = 10.144\,(\pm 0.0016) - 0.0497\,(\pm 0.0015) \times SST\,(°C) \tag{1}$$

The error on the intercept and slope for this regression equation corresponds to 1σ. The significant relationship between coral Sr/Ca records and instrumental SST ($r^2 = 0.71$, $p < 0.0001$, $n = 336$) supports the fidelity of coral Sr/Ca-SST relationship from the Xisha Islands. The slope value of $-0.0497$ mmol/mol°C$^{-1}$ is within the range of previous relationships derived for Pacific *Porites* spp., which ranged from $-0.04$ to $-0.12$ mmol/mol°C$^{-1}$ (Corrège, 2006; Sayani et al., 2019). To further validate the coral Sr/Ca thermometer, we applied this regression equation to another published modern Sr/Ca records from a *Porites* coral (15XS1), which were normalized against the international coral JCp-1 standard (Hathorne et al., 2013; Wang et al., 2018). 15XS1 was obtained from Qilianyu Reef (16°57′24.75″ N, 112°18′46.80″ E), approximately 13 km from our modern coral (Figure S3). The reconstructed SST from Qilianyu Reef were highly consistent with the instrumental SST from HadISST database for the period of 1990–2015 CE ($r = 0.81$, $p < 0.0001$, $n = 308$; Figure S9). Therefore, modern coral Sr/Ca records from the Xisha Islands establish the potential of *Porites* coral paleothermometry from the northern SCS for SST reconstruction.

### 4.4. Uncertainty Estimation

To fully account for the uncertainties in coral Sr/Ca-SST records, we included the analytical uncertainty of 0.016 mmol/mol (1σ) (Section 3.2), an estimate of the inter-colony uncertainty of 0.024 mmol/mol (1σ) in Sr/Ca among individual corals (Chen et al., 2018), and the calibration uncertainty associated with the coral Sr/Ca-SST equation (Section 4.3). The combined uncertainties were assessed using Monte Carlo simulations ($n = 1,000$; Carré et al., 2012; Lawman et al., 2020; Nurhati et al., 2011; see Supporting Information for further details). The uncertainties of the ensemble at a given time $t$ were evaluated using the root mean square error (RMSE) and defined as RMSE$_t$. The mean error of the entire record was calculated as the average of the RMSE$_t$ of the ensemble. For the monthly Sr/Ca-SST records from modern colony (YXN-1: 1980–2007 CE), the mean error was calculated to be 1.03°C (RMSE$_t$ ranging from 0.89°C to 1.15°C). Considering that our study primarily focused on interannual variability of the SSTA, we calculated the Sr/Ca-SSTA analogs

from the monthly analogs by subtracting the averaged annual cycle from the monthly Sr/Ca-SST series. Then, the RMSE$_t$ and the mean error of the Sr/Ca-SSTA ensemble were evaluated. The mean error of the Sr/Ca-SSTA records was calculated to be 0.32°C (RMSE$_t$ ranging from 0.30°C to 0.35°C). A 3–7-year band-pass filter was applied to the Sr/Ca-SSTA analogs to further evaluate the uncertainties of interannual variability. For the filtered Sr/Ca-SSTA records, the calculated uncertainty was reduced to 0.05°C (RMSE$_t$ ranging from 0.04°C to 0.06°C; Figure 4). Further, the error of sub-fossil coral record was estimated following the method for modern coral. The calculated mean error for sub-fossil coral record (GQ-2: 1149–1205 ± 4.9 (2$\sigma$) CE) was 0.98°C (RMSE$_t$ ranging from 0.81°C to 1.13°C) for the monthly Sr/Ca-SST series, 0.32°C (RMSE$_t$ ranging from 0.30°C to 0.39°C) for the Sr/Ca-SSTA series, and 0.05°C (RMSE$_t$ ranging from 0.04°C to 0.06°C) for the filtered Sr/Ca-SSTA series (Figure 5). Based on the uncertainty estimation of coral Sr/Ca-SST reconstruction, our results indicated reduced uncertainties in the SSTA as well as in the interannual signal relative to the monthly raw SST reconstructions.

## 5. Results and Discussion

### 5.1. Modern ENSO Variability

Instrumental SST variations around the Xisha Islands were characterized by prominent interannual variability for the period of 1900–2000 CE, with significant periodicities of 4.6 and 7.5 years (Figure S7a). To establish the expected response of SST to ENSO activity in this region, we calculated the ENSO detection skill for the period of 1900–2000 CE using SST records from Niño3.4 regions and the Xisha Islands. According to the empirically calibrated threshold techniques, El Niño (La Niña) events were defined by the SSTA in the Xisha Islands that exceeded 0.15°C (below −0.153°C). Based on this threshold level, the SST records from the Xisha Islands correctly identified 16 El Niño events and 11 La Niña events that were captured by Niño3.4 SST records for 1900–2000 CE, with a detection skill of 76% for El Niño events and 65% for La Niña events (Figure 4a). The number of false negatives was five El Niño events and six La Niña events. And the number of false positives was four El Niño events and three La Niña events (Figure 4a). Similarly, the SCS SST is sensitive to ENSO activity, with an ENSO detection skill (60%–70%) that is broadly similar to Niño3.4 region (Hereid, Quinn, & Okumura, 2013; Figure S10). The sliding variance with a 31-year window suggest that SST records from the Xisha Islands were characterized by increasing ENSO variability during the twentieth century (Figure 4b), which is consistent with ENSO variability patterns previously observed in Niño3.4 SST (Torrence & Compo, 1998; Trenberth, 1997). Therefore, we conclude that SST data from the SCS display a high sensitivity to ENSO activity and quantitatively reflect the changes in ENSO variability.

Spectral analysis of modern coral Sr/Ca-SST from the Xisha Islands also revealed significant periodicities from 2.9 to 4.5 years for the period of 1980–2007 CE (Figure S7b), similar to that of instrumental SST. To detect the interannual variability in regional coral Sr/Ca-SST, we compared the de-trended and filtered coral Sr/Ca with instrumental SST for 1,980–2007 CE. First, monthly anomalies of coral Sr/Ca and instrumental SST were obtained by subtracting the monthly means for the period of 1980–2007 CE. A significant correlation was detected between the 13-month running mean of coral Sr/Ca anomalies and Xisha SSTA ($r = -0.47$, $p_{adj} = 0.03$, $n_{eff} = 15$; Figure S11a). Furthermore, a 3–7-year band-pass filter was applied to the coral Sr/Ca anomalies and SSTA. We observed that ENSO variability between these two filtered series showed a significant negative correlation ($r = -0.76$, $p_{adj} = 0.008$, $n_{eff} = 8$; Figure S11b). Comparing the band-pass filtered Xisha coral Sr/Ca anomalies with other ENSO-sensitive coral records in which they overlap, we found our coral Sr/Ca anomalies exhibit significantly correlations with coral $\delta^{18}O$ anomalies from Kiritimati Island ($r = 0.68$, $p_{adj} = 0.029$, $n_{eff} = 8$; McGregor et al., 2013) and Palmyra Island ($r = 0.61$, $p_{adj} = 0.047$, $n_{eff} = 8$; Cobb et al., 2003), as well as coral Sr/Ca anomalies from Vanuatu ($r = -0.46$, $p_{adj} = 0.048$, $n_{eff} = 14$; Lawman et al., 2020; Figure S12). We further applied the ENSO threshold determined by instrumental SST to the modern coral Sr/Ca-SST reconstruction, with observations of five El Niño events and four La Niña events that were captured by Niño3.4 SST records from 1980 to 2007 CE (Figure 4e). The number of false negatives was two El Niño events and one La Niña events. And the number of false positives was three El Niño events and three La Niña events. The detection skill for El Niño events is 72% and for La Niña events is 80%. These results suggest that the SST revealed by coral Sr/Ca from the northern SCS is a sensitive and robust proxy for regional interannual variability and can provide the required benchmark for future coral paleo-ENSO
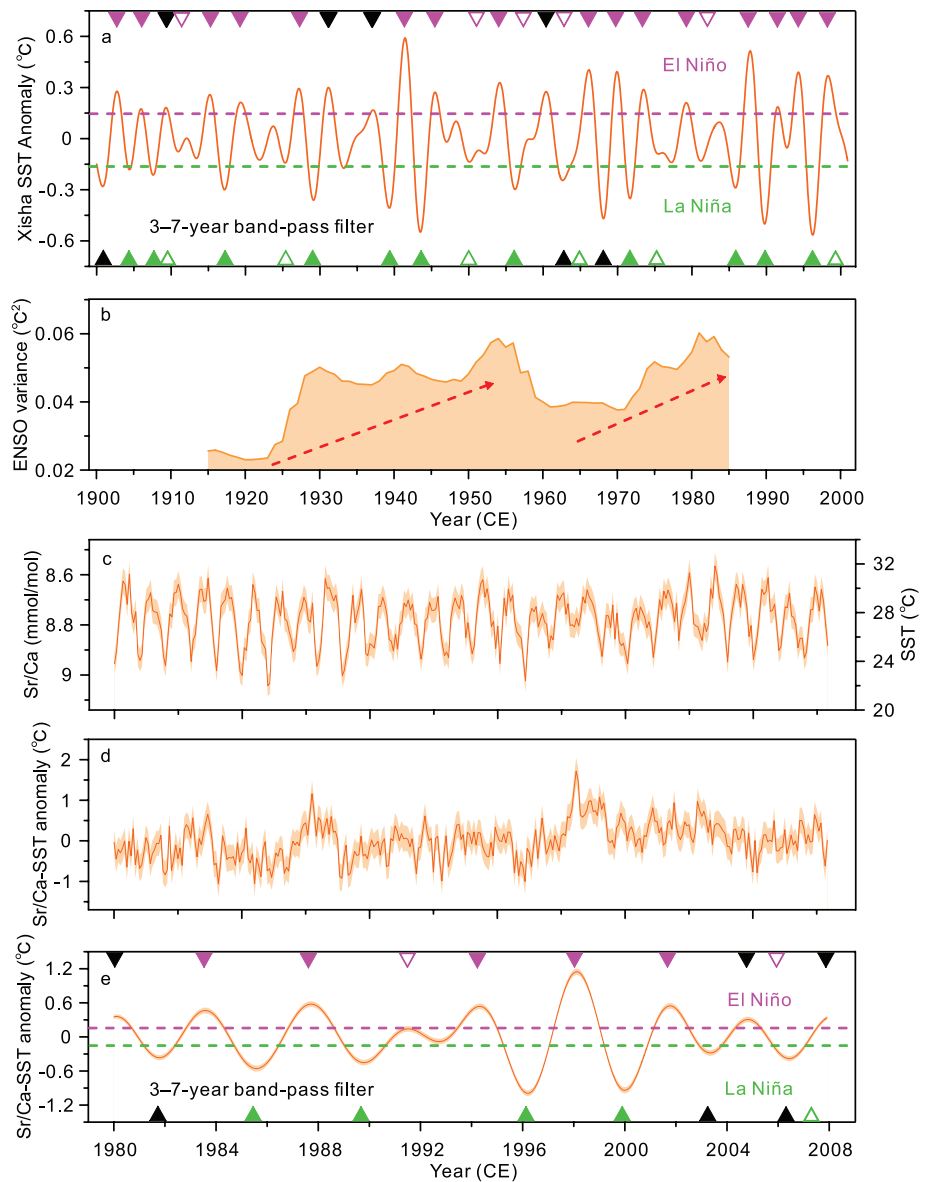
**Figure 4.** ENSO reconstruction based on instrumental SST (Rayner et al., 2003) from the Xisha Islands. (a) 3–7-year band-pass filtered instrumental SST anomalies for the period of 1900–2000 CE. (b) Variance in a sliding 31-year window for the 3–7-year band-pass filtered instrumental SST anomalies. Red arrow indicates increasing ENSO variability. (c) Monthly modern coral Sr/Ca records and SST reconstruction (dark orange) with Monte Carlo uncertainty quantification (light orange shading) that take analytical, inter-colony, and calibration uncertainty into account ($n = 1,000$ realizations). Coral Sr/Ca data are converted to SST using the Sr/Ca thermometer calibrated in this study. (d) SST anomalies reconstruction (dark orange) with uncertainty quantification (light orange shading). (e) 3–7-year band-pass filtered SST anomalies reconstruction (dark orange) with uncertainty quantification (light orange shading). Sections of the filtered SST anomalies that are above the empirical El Niño event threshold of 0.15°C (magenta dashed line) correspond to El Niño events. Similarly, sections of the filtered SST anomalies that fall below the empirical La Niña event threshold of −0.153°C (green dashed line) correspond to La Niña events. The solid magenta (green) triangles indicate the El Niño (La Niña) events captured by both the Xisha Islands SST and Niño3.4 SST. The hollow magenta (green) triangles indicate the El Niño (La Niña) events captured by Niño3.4 SST, but not identified in the Xisha Islands SST (false negatives). Black triangles represent ENSO events predicted by the Xisha Islands SST, but not identified in Niño3.4 SST (false positives). CE, Common Era; ENSO, El Niño–Southern Oscillation; SST, sea-surface temperature.
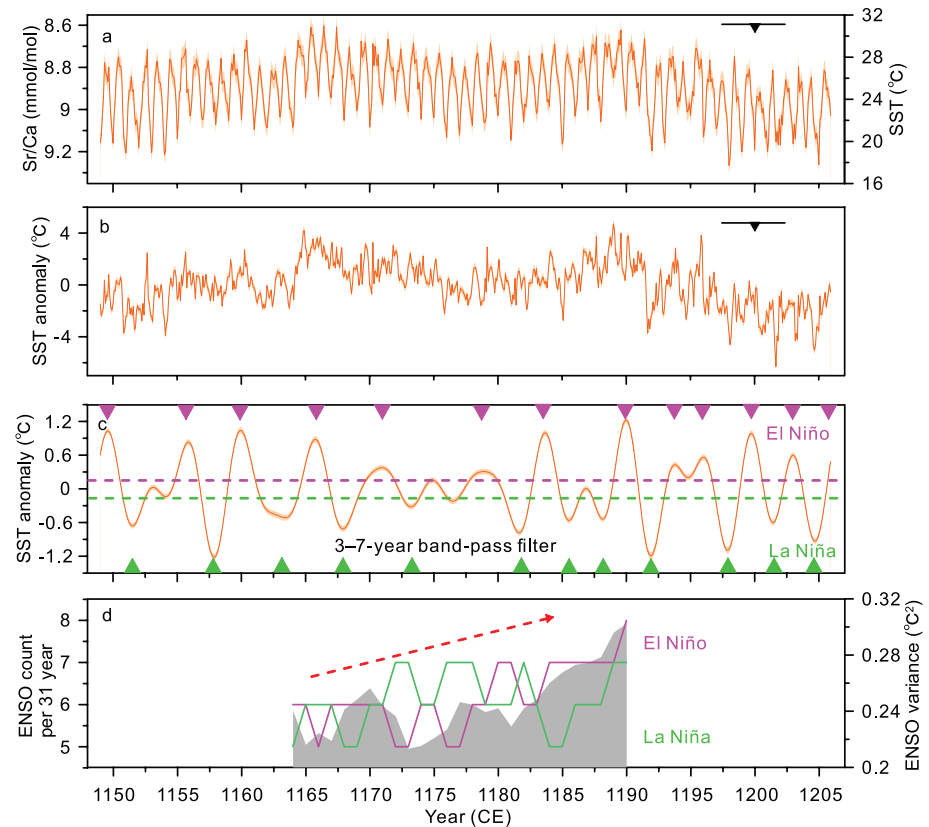
**Figure 5.** ENSO reconstruction based on sub-fossil coral Sr/Ca-SST from the Xisha Islands for the period of 1149–1205 ± 4.9 ($2\sigma$) CE. (a) Monthly sub-fossil coral Sr/Ca records and reconstructed SST (dark orange) with Monte Carlo uncertainty quantification (light orange shading) that take analytical, inter-colony, and calibration uncertainty into account ($n = 1,000$ realizations). (b) SST anomalies reconstruction (dark orange) with uncertainty quantification (light orange shading). (c) 3–7-year band-pass filtered SST anomalies reconstruction (dark orange) with uncertainty quantification (light orange shading). Sections of the filtered SST anomalies that are above the empirical El Niño event threshold of 0.15°C (magenta dashed line) correspond to predicted El Niño events (magenta triangles). Similarly, sections of the filtered SST anomalies that fall below the empirical La Niña event threshold of −0.153°C (green dashed line) correspond to predicted La Niña events (green triangles). (d) The number of El Niño (magenta line) and La Niña (green line) events in a sliding 31-year window. Gray shading is the variance in a sliding 31-year window for the filtered SST anomalies. Red dashed arrow indicates intensified ENSO variability and increased frequency of El Niño events. Black triangles with horizontal bar mark the $^{230}$Th age of 1200.1 ± 4.9 ($2\sigma$) CE for sub-fossil coral. CE, Common Era; ENSO, El Niño–Southern Oscillation; SST, sea-surface temperature.

reconstructions. We subsequently applied the empirically calibrated ENSO threshold to the sub-fossil coral Sr/Ca-SST records from the Xisha Islands.

### 5.2. Reconstruction of ENSO Activity During the MCA

Seasonal fluctuations are notable in sub-fossil coral Sr/Ca series, with clear annual cycles over the 57-year record (Figure 5a). Spectral analyses of this Sr/Ca-SST records revealed pronounced interannual peak of 3.3 years from 1149 to 1205 ± 4.9 ($2\sigma$) CE (Figure S7c). To further examine the ENSO variability, we applied a 3–7-year band-pass filter to the monthly coral Sr/Ca-SSTA obtained by subtracting the monthly means for 1149–1205 ± 4.9 ($2\sigma$) CE (Figure 5b). The total variance of filtered sub-fossil coral Sr/Ca-SSTA (0.29°C$^2$) shows relatively stronger than that of modern coral (0.19°C$^2$), suggesting ENSO variability at 1,149–1,205 ± 4.9 ($2\sigma$) CE was enhanced by 53% compared with today (Figure S13). According to the empirically determined ENSO threshold (see Section 5.1), we observed approximately 13 predicted El Niño events and 12 predicted La Niña events from 1149 to 1205 ± 4.9 ($2\sigma$) CE (Figure 5c). The ENSO variations throughout this time interval were evaluated by counting the ENSO events using a 31-year sliding window

(Cobb et al., 2003; Han et al., 2020). The larger variations in the frequency of El Niño events during 31-year periods relative to that of La Niña events (Figure 5d) indicated that El Niño events play a leading role in the variations of ENSO variability.

A plethora of evidence indicates there are discrepancies in the reconstruction of ENSO activity during the MCA. Lake sediments from Laguna Pallcacocha (Moy et al., 2002) and Galápagos Islands (Conroy et al., 2008) demonstrate more frequent and stronger El Niño events during the MCA. Speleothem $\delta^{18}O$ records from the northeastern Peru (Reuter et al., 2009), the Isthmus of Panama (Lachniet et al., 2004), and the western Pacific (Tan et al., 2019; Tierney et al., 2010) document relatively decreased rainfall and dry climate episodes from 950 to 1250 CE, which is consistent with the paradigm of persistent El Niño pattern in this region (Toth et al., 2015). However, the MCA has been characterized by persistently weak El Niño activity based on marine sediment cores from offshore Peru (Fleury et al., 2015; Rein et al., 2005) and basin ventilation records from Indonesia (Langton et al., 2008). Extreme rainfall in the northwestern Australia (Dennistona et al., 2015) and aridity in the western North America (Cook et al., 2004; Graham et al., 2007; Li et al., 2011) also suggest enhanced La Niña activity from 850 to 1450 CE, which is supported by SST reconstructions from the central (Cobb et al., 2003; Seager et al., 2008) and eastern (Conroy et al., 2010) equatorial Pacific.

Several factors may have contributed to the observed discrepancies in reconstruction of ENSO activity during the MCA. A growing body of evidence suggests that the ENSO teleconnection patterns may have undergone significant reorganization in the tropical oceanic–atmospheric circulation system during this period (Graham et al., 2011; Lachniet et al., 2004; Rein et al., 2005), which may have affected regional precipitation in the tropical Pacific and produced ENSO-driven patterns of SST and rainfall that were different than at present. For example, sediment records from Laguna Pallcacocha indicate large amounts of precipitation associated with increased El Niño episodes during the medieval period (Moy et al., 2002). However, this interpretation is contradicted by records of reduced rainfall in the western United States, where precipitation patterns are similar to northwestern South America at present (Graham et al., 2007). In addition, the North American Drought Atlas (Cook et al., 2004) depicts shifts in North American hydroclimate from the MCA to the Little Ice Age (LIA) consistent with changes in the ENSO-United States teleconnection (Li et al., 2011).

An alternative explanation for the disagreement in ENSO activity during the MCA could, therefore, be related to the inconsistency in the time period used to represent the medieval period in paleo-records. For example, the enhanced La Niña activity in the tropical Pacific suggested by corals from Palmyra Atoll during the MCA were from the period of 1320–1462 CE (Seager et al., 2008). However, this time interval has often been defined as the transitional stage from the MCA to the LIA (Masson-Delmotte et al., 2013) and was likely characterized by an evolution in ENSO behavior.

### 5.3. Intensified ENSO Variability for the Late MCA

Despite numerous studies shedding light on ENSO variability relative to modern times (Moy et al., 2002; Rein et al., 2005), our records allow for testing the hypothesis that ENSO variability likely changed over the course of the MCA. The results of 31-year sliding variance suggest a lower variance from 1149 to 1179 ± 4.9 ($2\sigma$) CE and a higher variance from 1180 to 1205 ± 4.9 ($2\sigma$) CE (Figure 5d), which is consistent with the change in the number of El Niño events. Given that the MCA extends over 300 years from 950 to 1250 CE (Masson-Delmotte et al., 2013), the time interval of 1149–1205 ± 4.9 ($2\sigma$) CE falls within the late MCA. The transition of ENSO variability from weak to strong during 1149–1205 ± 4.9 ($2\sigma$) CE suggests intensified ENSO variability during the late MCA. Coral oxygen isotopic records from Palmyra Islands also exhibit significant changes in the decadal ENSO behavior in the twelfth century (Cobb et al., 2003). We applied the same sliding variance used in this study to the filtered coral $\delta^{18}O$ anomalies from 1149 to 1220 ± 5 ($2\sigma$) CE. This record also suggests less variance from 1149 to 1179 ± 5 ($2\sigma$) CE and more variance from 1180 to 1220 ± 5 ($2\sigma$) CE (Figure S14). The similar changes in variability in the records from both the Xisha Islands and the central Pacific provides strong evidence for intensified ENSO variability during the late MCA (Figure 6a).

Another coral Sr/Ca from Vanuatu in the southwest Pacific provide insights into ENSO variability from 1051 to 1150 ± 2.7 ($2\sigma$) CE, a period coincident with the middle MCA (Lawman et al., 2020). Applying the
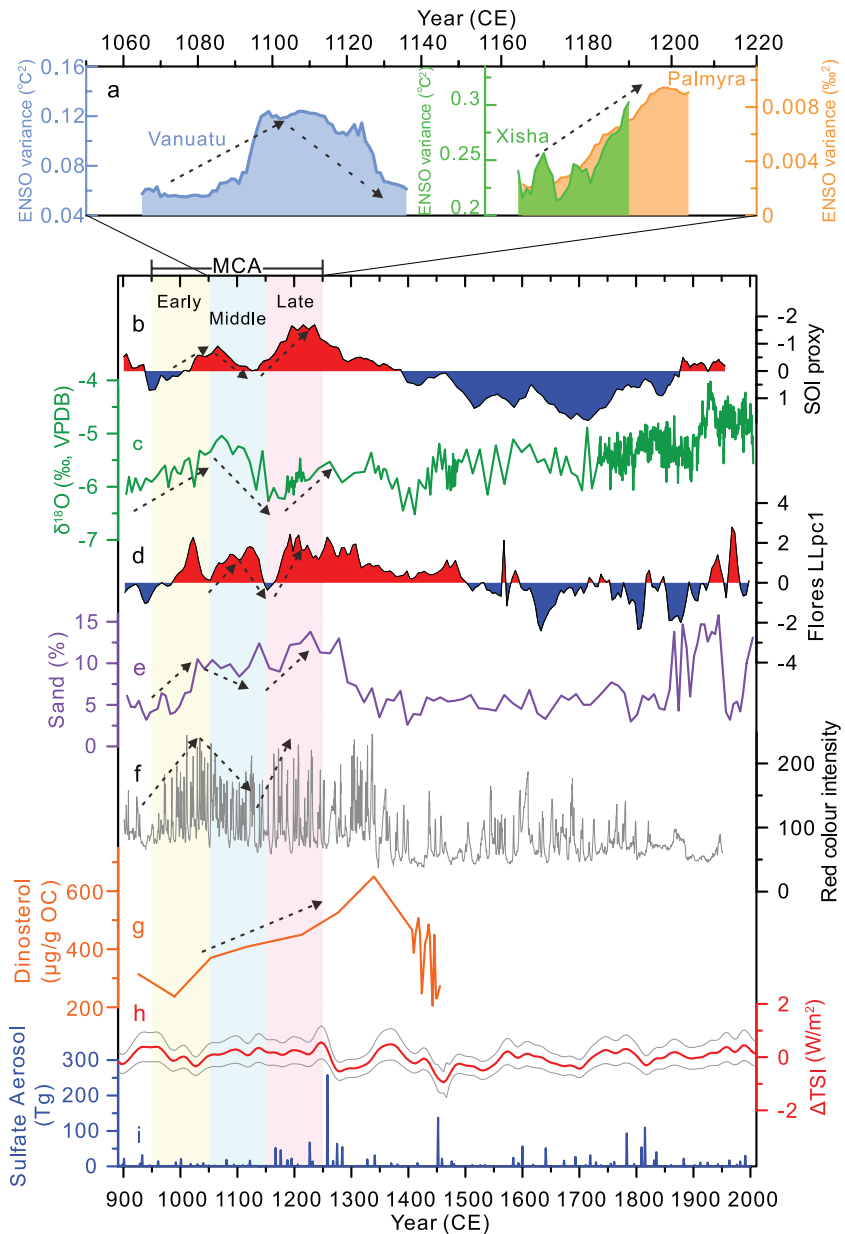
**Figure 6.** ENSO reconstruction based on various proxies from the tropical Pacific during the Medieval Climate Anomaly (MCA). (a) Variance in a sliding 31-year window for the filtered coral Sr/Ca-SST anomalies from Vanuatu for the period of 1050–1151 ± 2.7 (2σ) CE (blue shading; Lawman et al., 2020), the filtered coral Sr/Ca-SST anomalies from the Xisha Islands for the period of 1149–1205 ± 4.9 (2σ) CE (green shading), and the filtered coral δ18O anomalies from Palmyra Island for the period of 1149–1220 ± 5 (2σ) CE (orange shading; Cobb et al., 2003). (b) Reconstructed Southern Oscillation Index-like records (Yan et al., 2011). (c) Stalagmite δ18O records from the southern Thailand (Tan et al., 2019). (d) Multiproxy synthesized stalagmite records from the eastern Indonesia (Griffiths et al., 2016). (e) Percent of sand in lake sediments from El Junco in Galápagos (Conroy et al., 2008). (f) Red color intensity of sedimentation in Laguna Pallcacocha, Ecuador (Moy et al., 2002). (g) Dinosterol abundance from Peru (Makou et al., 2010). (h) Total solar irradiance (TSI) with the uncertainty (1σ, gray lines) based on the cosmogenic radionuclide [10]Be (Steinhilber et al., 2009). (i) Global volcanic sulfate aerosol injection (Gao et al., 2008). Yellow, blue, and pink vertical fields indicate the approximate intervals for the early (950–1050 CE), middle (1051–1150 CE), and late (1151–1250 CE) MCA, respectively. Black dashed arrows indicate the trend of intensified or diminished ENSO variability and El Niño activity. CE, Common Era; ENSO, El Niño–Southern Oscillation; MCA, Medieval Climate Anomaly; SST, sea-surface temperature; TSI, Total solar irradiance.

sliding variance with a 31-year window to the filtered coral Sr/Ca-SSTA from Vanuatu, we found that the period of 1051–1099 ± 2.7 (2σ) CE experienced more variability while the period of 1100–1150 ± 2.7 (2σ) CE had less variability (Figure S15). These results indicate a transition from enhanced to reduced ENSO variability for the middle MCA (Figure 6a). Combined with the intensified ENSO variability for the late MCA, coral records across the tropical Pacific portray sustained changes in ENSO during the MCA, with interannual SST variability fluctuating between intervals with more and less variability.

There is a lack of additional records on ENSO variability for the MCA due to the limited temporal resolutions that characterize most proxy reconstructions. However, considering that the intensified ENSO variability is consistent with the enhanced number of El Niño events (Figure 5d), the transition from enhanced to reduced ENSO variability during the middle MCA and intensified ENSO variability during the late MCA is supported by several other proxy reconstructions of El Niño activity across the tropical Pacific. A reconstruction of the Southern Oscillation Index (SOI) shows the decreasing trend in El Niño activity from 1,052 to 1149 CE and continuously increasing El Niño activity from 1,150 to 1200 CE (Yan et al., 2011; Figure 6b). The increased δ$^{18}$O in stalagmite records from the southern Thailand suggest decreased rainfall and dry climate episodes in the central Indo-Pacific from 950 to 1050 CE and 1,151 to 1250 CE, resembling enhanced El Niño activity. In contrast, decreased stalagmite δ$^{18}$O with attenuated El Niño activity occurred from 1,051 to 1150 CE (Tan et al., 2019; Figure 6c). Composite speleothem records from the southeastern Indonesia also demonstrate an enhanced to reduced transition in El Niño activity during the middle MCA and intensified El Niño activity during the late MCA (Griffiths et al., 2016; Figure 6d). In the eastern Pacific, lake sediment records from El Junco in Galápagos Islands imply increased precipitation and intensified El Niño activity during the early and late MCA, and decreased precipitation and attenuated El Niño activity during the middle MCA (Conroy et al., 2008; Figure 6e). Similarly, sedimentation records from Laguna Pallcacocha in the southern Ecuador indicate an increased red color intensity during the early and late MCA, corresponding to intensified El Niño activity and more frequent ENSO events (Moy et al., 2002; Figure 6f). Furthermore, biomarkers from marine sediments off the Peruvian coast suggest that the late MCA coincides with an interval of increased dinosterol abundance and enhanced El Niño activity (Makou et al., 2010; Figure 6g). Although there is some temporal disagreement on the evolutionary characteristics of ENSO variability throughout the MCA owing to differences in chronology and temporal resolution, the general correspondence between these ENSO reconstructions and coral records from the tropical Pacific supports the conclusion of fluctuating ENSO variability during the MCA and intensified ENSO variability during the late MCA.

### 5.4. Internally-Driven ENSO Variability

The coherent evolutionary characteristics of ENSO activity and intensified ENSO variability during the late MCA allow for an assessment of the mechanisms driving ENSO variability. Currently, one of the controversies about ENSO dynamics is the response of ENSO variability to external climate forcing induced by solar irradiance and volcanism over the last millennium (Cobb et al., 2003; Mann et al., 2009). Although formal attribution analyses have not been performed, we found a lack of consistent response of ENSO variability to external climate forcing. For example, intensified ENSO variability was not accompanied by relatively decreased solar irradiance (Figure 6h) or increased volcanism (Figure 6i), which indicates that larger ENSO variability occurred without strong external climate forcing. While our results suggest that ENSO variability showed significant fluctuations throughout the MCA, the amplitude of the total solar irradiance had relatively low variability during this period (Steinhilber et al., 2009; Figure 6h). Similarly, a comparison of ENSO variability with global volcanic activity (Gao et al., 2008) revealed a lack of coherent temporal correspondence with ENSO activity following large volcanic eruptions (Figure 6i). Moreover, the magnitude of external climate forcing during the MCA, including orbital factors (Bertrand et al., 2002), solar activity (Steinhilber et al., 2009), and volcanism (Gao et al., 2008) did not differ significantly from that of modern and preindustrial climate forcing (Bradley et al., 2003, 2016), but ENSO variability at 1149–1205 ± 4.9 (2σ) CE was enhanced by 53% compared with today (Figure S13). Therefore, we suggest that the ENSO variability during the MCA was likely driven by the internal variability of the climate system.

Other paleoclimate studies have also concluded that there is little evidence of a response of ENSO variability to external forcing during other periods over the last millennium. For example, coral δ$^{18}$O records from Palmyra Island revealed little correspondence between ENSO variability and solar or volcanic forcing,

which implies that ENSO activity changed markedly in the absence of apparent external forcing (Cobb et al., 2003). Data-model comparisons have also revealed that numerous model simulations may overestimate the sensitivity of ENSO variability to volcanic forcing (Dee et al., 2020). A spliced fossil coral $\delta^{18}$O record from Misima Island in the western Pacific demonstrated reduced El Niño variability relative to the modern era, that had no apparent connection to solar forcing, instead likely arose from unforced internal dynamics (Hereid, Quinn, Taylor, et al., 2013). A 2000-year control simulation exhibited a strong interdecadal and intercentennial modulation in ENSO behavior under constant boundary conditions. This simulation also indicated that the intervals of varying ENSO behavior can stem purely from stochastic processes within the climate system (Wittenberg, 2009). In addition, other long, unforced integrations of preindustrial control climate model runs exhibited a broad ENSO variability range (Deser et al., 2012). These results indicate that a range of ENSO behavior can occur in the absence of external forcing and that the internal dynamics of the climate system play a prominent role in modulating ENSO variability. Therefore, a large body of evidence supports our hypothesis that fluctuating ENSO variability during the MCA and intensified ENSO variability during the late MCA, as observed in the tropical Pacific proxy reconstructions, most likely resulted from internal variability of the climate system. Considering the sensitivity of ENSO variability to anthropogenic forcing (Cobb et al., 2013), internally generated modulations in ENSO activity will further complicate external perturbations.

## 6. Conclusions

In this study, ENSO variability during the late MCA was investigated using monthly coral Sr/Ca-SST records from the Xisha Islands in the northern SCS. The instrumental SST from the northern SCS revealed that the ENSO detection skills are similar to those for Niño3.4 regions and accurately record the changes in ENSO variability. Moreover, coral Sr/Ca-SST from the Xisha Islands serve as sensitive and robust proxies for ENSO variability. We applied an empirically determined threshold to sub-fossil coral Sr/Ca-SST records and determined El Niño events dominated the variations of ENSO variability from 1149 to 1205 ± 4.9 ($2\sigma$) CE. Comparisons of our results with other ENSO-sensitive proxy reconstructions show that the discrepancies among records regarding ENSO activity during the MCA may be related to the reorganized ENSO teleconnection pattern and the varied ENSO activity during different periods of the MCA. The coral Sr/Ca-SST records developed in this study, in combination with other proxy reconstructions from the tropical Pacific, supported fluctuating ENSO variability during the MCA and intensified ENSO variability during the late MCA. Given that external climate forcing was minimal throughout the MCA and there was a lack of a coherent temporal correspondence between solar irradiance or volcanic eruptions and ENSO activity, we hypothesize that internal dynamics of the climate system plays a prominent role in modulating ENSO variability. These observations significantly advance our understanding of the ENSO variability during the MCA and provide insight into the forcing of ENSO phenomena. Nonetheless, high-resolution reconstructions of ENSO activity from other locations are required to achieve a comprehensive understanding of the changes in ENSO activity.

## Data Availability Statement

Supporting data for this study are available in the Zenodo data repository, doi: https://doi.org/10.5281/zenodo.4584183.

## References

Alexander, M. A., Bladé, I., Newman, M., Lanzante, J. R., Lau, N. C., Scott, J. D., et al. (2002). The atmospheric bridge: The influence of ENSO teleconnections on air–sea interaction over the global oceans. *Journal of Climate*, *15*(16), 2205–2231. https://doi.org/10.1175/1520-0442(2002)015<2205:tabtio>2.0.co;2

Alibert, C., & McCulloch, M. T. (1997). Strontium/calcium ratios in modern *Porites* corals from the great barrier reef as a proxy for sea surface temperature: Calibration of the thermometer and monitoring of ENSO. *Paleoceanography*, *12*(3), 345–363. https://doi.org/10.1029/97pa00318

Beck, J. W., Edwards, R. L., Ito, E., Taylor, F. W., Recy, J., Rougerie, F., et al. (1992). Sea-surface temperature from coral skeletal strontium/calcium ratios. *Science*, *257*(5070), 644–647. https://doi.org/10.1126/science.257.5070.644

Bertrand, C., Loutre, M. F., Crucifix, M., & Berger, A. (2002). Climate of the last millennium: A sensitivity study. *Paleoceanography*, *52A*, 221–244. https://doi.org/10.1034/j.1600-0870.2002.00287.x

Bohonak, A. J. (2004). *RMA: Software for reduced major axis regression*. Retrieved from http://www.bio.sdsu.edu/pub/andy/RMA.html

Booth, R., Notaroa, M., Jacksonb, S. T., & Kutzbacha, J. E. (2006). Widespread drought episodes in the western Great Lakes region during the past 2000 years: Geographic extent and potential mechanisms. *Earth and Planetary Science Letters*, *242*(3–4), 415–427. https://doi.org/10.1016/j.epsl.2005.12.028

Box, G. E. P., Jenkins, G. M., & Reinsel, G. C. (1976). *Time series analysis: Forecasting and control* (Vol. 16). (Holden-Day San Francisco).

Bradley, R. S., Hughes, M. K., & Diaz, H. F. (2003). Climate change: Climate in medieval time. *Science*, *302*(5644), 404–405. https://doi.org/10.1126/science.1090372

Bradley, R. S., Wanner, H., & Diaz, H. F. (2016). The medieval quiet period. *The Holocene*, *26*(6), 1–4. https://doi.org/10.1177/0959683615622552

Cai, W., Borlace, S., Lengaigne, M., Rensch, P. v., Collins, M., Vecchi, G., et al. (2014). Increasing frequency of extreme El Niño events due to greenhouse warming. *Nature Climate Change*, *4*(2), 111–116. https://doi.org/10.1038/nclimate2100

Carré, M., Sachs, J. P., Wallace, J. M., & Favier, C. (2012). Exploring errors in paleoclimate proxy reconstructions using Monte Carlo simulations: Paleotemperature from mollusk and coral geochemistry. *Climate of the Past*, *8*, 433–450. https://doi.org/10.5194/cp-8-433-2012

Charles, C. D., Hunter, D. E., & Fairbanks, R. G. (1997). Interaction between the ENSO and the Asian Monsoon in a coral record of tropical climate. *Science*, *277*(15), 925–928. https://doi.org/10.1126/science.277.5328.925

Chen, T., Cobb, K. M., Roff, G., Zhao, J., Yang, H., Hu, M., & Zhao, K. (2018). Coral-derived western Pacific tropical sea surface temperatures during the last millennium. *Geophysical Research Letters*, *45*(8), 3542–3549. https://doi.org/10.1002/2018gl077619

Clement, A. C., Seager, R., Cane, M. A., & Zeblak, S. E. (1996). An ocean dynamical thermostat. *Journal of Climate*, *9*(9), 2190–2196. https://doi.org/10.1175/1520-0442(1996)009<2190:aodt>2.0.co;2

Cobb, K. M., Charles, C. D., Cheng, H., & Edwards, R. L. (2003). El Niño/Southern Oscillation and tropical Pacific climate during the last millennium. *Nature*, *424*(6946), 271–276. https://doi.org/10.1038/nature01779

Cobb, K. M., Westphal, N., Sayani, H. R., Watson, J. T., Lorenzo, E. D., Cheng, H., et al. (2013). Highly variable El Niño–Southern Oscillation throughout the Holocene. *Science*, *339*(6115), 67–70. https://doi.org/10.1126/science.1228246

Cole, J. E., Fairbanks, R. G., & Shen, G. T. (1993). Recent variability in the Southern Oscillation: Isotopic results from a Tarawa Atoll coral. *Science*, *260*, 1790–1793. https://doi.org/10.1126/science.260.5115.1790

Conroy, J. L., Overpeck, J. T., & Cole, J. E. (2010). El Niño/Southern Oscillation and changes in the zonal gradient of tropical Pacific sea surface temperature over the last 1.2 ka. In *Proceedings of the national academy of sciences news* (*18*(1), pp. 32–34). https://doi.org/10.22498/pages.18.1.32

Conroy, J. L., Restrepo, A., Overpeck, J. T., Kannan, M. S., Cole, J. E., Bush, M. B., et al. (2008). Unprecedented recent warming of surface temperatures in the eastern tropical Pacific Ocean. *Nature Geoscience*, *2*(1), 46–50. https://doi.org/10.1038/ngeo390

Cook, E. R., Woodhouse, C. A., Eakin, C. M., Meko, D. M., & Stahle, D. W. (2004). Long-term aridity changes in the western United States. *Science*, *306*(5698), 1015–1018. https://doi.org/10.1126/science.1102586

Corrège, T. (2006). Sea surface temperature and salinity reconstruction from coral geochemical tracers. *Palaeogeography, Palaeoclimatology, Palaeoecology*, *232*(2–4), 408–428. https://doi.org/10.1016/j.palaeo.2005.10.014

Corrège, T., Delcroix, T., Récy, J., Beck, W., Cabioch, G., & Cornec, F. L. (2000). Evidence for stronger El Niño–Southern Oscillation (ENSO) events in a mid-holocene massive coral. *Paleoceanography*, *15*(4), 465–470. https://doi.org/10.1029/1999pa000409

D'Arrigo, R., Cook, E. R., Wilson, R. J., Allan, R., & Mann, M. E. (2005). On the variability of ENSO over the past six centuries. *Geophysical Research Letters*, *32*, L03711. https://doi.org/10.1029/2004GL022055

Dee, S. G., Cobb, K. M., Emile-Geay, J., Ault, T. R., Edwards, R. L., Cheng, H., & Charles, C. D. (2020). No consistent ENSO response to volcanic forcing over the last millennium. *Science*, *367*(6485), 1477–1481. https://doi.org/10.1126/science.aax2000

DeLong, K. L., Quinn, T. M., Taylor, F. W., Shen, C. C., & Lin, K. (2013). Improving coral- base paleoclimate reconstructions by replicating 350 years of coral Sr/Ca variations. *Palaeogeography, Palaeoclimatology, Palaeoecology*, *373*, 6–24. https://doi.org/10.1016/j.palaeo.2012.08.019

Dennistona, R. F., Villarinib, G., Gonzalesa, A. N., Wyrwollc, K., Polyakd, V. J., Ummenhofere, C. C., et al. (2015). Extreme rainfall activity in the Australian tropics reflects changes in the El Niño/Southern Oscillation over the last two millennia. In *Proceedings of the national academy of sciences* (*112*(15), pp. 4576–4581). http://doi.org/10.1073/pnas.1422270112

Deser, C., Phillips, A. S., Tomas, R. A., Okumura, Y. M., Alexander, M. A., Capotondi, A., et al. (2012). ENSO and Pacific decadal variability in the community climate system model version 4. *Journal of Climate*, *25*, 2622–2651. https://doi.org/10.1175/jcli-d-11-00301.1

Diaz, H. F., & Markgraf, V. (2000). *El Niño and the southern OscillationMultiscale variability and global and regional impacts*. Cambridge, United Kingdom: Cambridge University: Press.

Emile-Geay, J., Cobb, K. M., Mann, M. E., & Wittenberg, A. T. (2013a). Estimating central equatorial Pacific SST variability over the past millennium. Part I: Methodology and validation. *Journal of Climate*, *26*(7), 2302–2328. https://doi.org/10.1175/JCLI-D-11-00510.1

Emile-Geay, J., Cobb, K. M., Mann, M. E., & Wittenberg, A. T. (2013b). Estimating central equatorial Pacific SST variability over the past millennium. Part II: Reconstructions and implications. *Journal of Climate*, *26*(7), 2329–2352. https://doi.org/10.1175/JCLI-D-11-00511.1

Fairbanks, R. G., & Dodge, R. E. (1979). Annual periodicity of the $^{18}O/^{16}O$ and $^{13}C/^{12}C$ ratios in the coral Montastrea annularis. *Geochimica et Cosmochimica Acta*, *43*, 1009–1020. https://doi.org/10.1016/0016-7037(79)90090-5

Felis, T., Pätzold, J., Loya, Y., Fine, M., Nawar, A. H., & Wefer, G. (2000). A coral oxygen isotope record from the northern Red Sea documenting NAO, ENSO, and North Pacific teleconnections on Middle East climate variability since the year 1750. *Paleoceanography*, *15*, 679–694. https://doi.org/10.1029/1999pa000477

Fleury, S., Martinez, P., Crosta, X., Charlier, K., Billy, I., Hanquiez, V., et al. (2015). Pervasive multidecadal variations in productivity within the peruvian upwelling system over the last millennium. *Quaternary Science Reviews*, *125*, 78–90. https://doi.org/10.1016/j.quascirev.2015.08.006

Gagan, M. K., Ayliffe, L. K., Hopley, D., Cali, J. A., Mortimer, G. E., Chappell, J., et al. (1998). Temperature and surface-ocean water balance of the mid-Holocene tropical western pacific. *Science*, *279*(5353), 1014–1018. https://doi.org/10.1126/science.279.5353.1014

Gao, C., Robock, A., & Ammann, C. (2008). Volcanic forcing of climate over the past 1500 years: An improved ice core-based index for climate models. *Journal of Geophysical Research*, *113*, D23111. https://doi.org/10.1029/2008jd010239

Ghil, M., Allen, M. R., Dettinger, M. D., Ide, K., Kondrashov, D., Mann, M. E., et al. (2002). Advanced spectral methods for climatic time series. *Reviews of Geophysics*, *40*(1). https://doi.org/10.1029/2000rg000092

Goodwin, I. D., Browning, S., Lorrey, A. M., Mayewski, P. A., Phipps, S. J., Bertler, N. A. N., et al. (2014). A reconstruction of extratropical Indo-Pacific sea-level pressure patterns during the Medieval Climate Anomaly. *Climate Dynamics*, *43*(5–6), 1197–1219. https://doi.org/10.1007/s00382-013-1899-1

Graham, N. E., Ammann, C. M., Fleitmann, D., Cobb, K. M., & Luterbacher, J. (2011). Support for global climate reorganization during the "Medieval Climate Anomaly". *Climate Dynamics*, *37*, 1217–1245. https://doi.org/10.1007/s00382-010-0914-z

Graham, N. E., Hughes, M. K., Ammann, C. M., Cobb, K. M., Hoerling, M. P., Kennett, D. J., et al. (2007). Tropical Pacific–mid-latitude teleconnections in medieval times. *Climatic Change*, *83*(1–2), 241–285. https://doi.org/10.1007/s10584-007-9239-2

Griffiths, M. L., Kimbrough, A. K., Gagan, M. K., Drysdale, R. N., Cole, J. E., Johnson, K. R., et al. (2016). Western pacific hydroclimate linked to global climate variability over the past two millennia. *Nature Communications*, *7*, 11719. https://doi.org/10.1038/ncomms11719

Guo, Q., & Wang, R. (1990). The relationship between the winter monsoon activity over East Asian and the El Niño events. *Acta Geographica Sinica*, *45*(1), 68–77. https://doi.org/10.1007/s00376-011-0014-y(in Chinese with English abstract).

Han, T., Yu, K. F., Yan, H., Jiang, W., Yan, H. Q., & Tao, S. C. (2020). Coral δ18O-based reconstruction of El Niño-Southern Oscillation from the northern South China Sea since 1851 AD. *Quaternary International*, *32*(4). https://doi.org/10.1016/j.quaint

Hathorne, E. C., Gagnon, A., Felis, T., Adkins, J., Asami, R., Boer, W., et al. (2013). Interlaboratory study for coral Sr/Ca and other element/Ca ratio measurements. *Geochemistry, Geophysics, Geosystems*, *14*(9), 3730–3750. https://doi.org/10.1002/ggge.20230

Hereid, K. A., Quinn, T. M., & Okumura, Y. M. (2013). Assessing spatial variability in El Niño-Southern Oscillation event detection skill using coral geochemistry. *Paleoceanography*, *28*(1), 14–23. https://doi.org/10.1029/2012pa002352

Hereid, K. A., Quinn, T. M., Taylor, F. W., Shen, C. C., Edwards, R. L., & Cheng, H. (2013). Coral record of reduced El Niño activity in the early 15th to middle 17th centuries. *Geology*, *41*(1), 51–54. https://doi.org/10.1130/g33510.1

Hu, Y., Sun, X., Cheng, H., & Yan, H. (2020). Evidence from giant-clam δ18O of intense El Niño–Southern Oscillation-related variability but reduced frequency 3700 years ago. *Climate of the Past*, *16*, 597–610. https://doi.org/10.5194/cp-16-597-2020

Klein, S. A., Soden, B. J., & Lau, N. (1999). Remote sea surface temperature variations during ENSO: Evidence for a tropical atmospheric bridge. *Journal of Climate*, *12*(4), 917–932. https://doi.org/10.1175/1520-0442(1999)012<0917:rsstvd>2.0.co;2

Lachniet, M. S., Bums, S. J., Pipemo, D. R., Asmerom, Y., Polyak, V. J., Moy, C. M., & Christenson, K. (2004). A 1500-year El Niño/Southern Oscillation and rainfall history for the Isthmus of Panama from speleothem calcite. *Journal of Geophysical Research*, *109*(20). https://doi.org/10.1029/2004jd004694

Langton, S. J., Linsley, B. K., Robinson, R. S., Rosenthal, Y., Oppo, D. W., Eglinton, T. I., et al. (2008). 3500 yr record of centennial-scale climate variability from the western pacific warm pool. *Geology*, *36*(10), 795–798. https://doi.org/10.1130/g24926a.1

Larkin, N. K., & Harrison, D. E. (2005). On the definition of El Niño and associated seasonal average U.S. weather anomalies. *Geophysical Research Letters*, *33*(12), L12604. https://doi.org/10.1029/2005GL022738

Lawman, A. E., Quinn, T. M., Partin, J. W., Thirumalai, K., Taylor, F. W., Wu, C.-C., et al. (2020). A century of reduced ENSO variability during the Medieval Climate Anomaly. *Paleoceanography and Paleoclimatology*, *35*, e2019PA003742. https://doi.org/10.1029/2019pa003742

Ledru, M. P., Jomelli, V., Samaniego, P., Vuille, M., Hidalgo, S., Herrera, M., & Ceron, C. (2013). The Medieval Climate Anomaly and the Little Ice Age in the eastern Ecuadorian Andes. *Climate of the Past*, *9*(1), 307–321. https://doi.org/10.5194/cp-9-307-2013

Li, J. B., Xie, S. P., Cook, E. R., Huang, G., D'Arrigo, R., Liu, F., et al. (2011). Interdecadal modulation of El Niño amplitude during the past millennium. *Nature Climate Change*, *1*(2), 114–118. https://doi.org/10.1038/nclimate1086

Makou, M. C., Eglinton, T. I., Oppo, D. W., & Hughen, K. A. (2010). Postglacial changes in El Niño and La Niña behavior. *Geology*, *38*(1), 43–46. https://doi.org/10.1130/g30366.1

Mann, M. E., Zhang, Z., Rutherford, S., Bradley, R. S., Hughes, M. K., Shindell, D., et al. (2009). Global signatures and dynamical origins of the Little Ice Age and Medieval climate anomaly. *Science*, *326*(5957), 1256–1260. https://doi.org/10.1126/science.1177303

Marshall, J. F., & McCulloch, M. T. (2002). An assessment of the Sr/Ca ratio in shallow water hermatypic corals as a proxy for sea surface temperature. *Geochimica et Cosmochimica Acta*, *66*, 3263–3280. https://doi.org/10.1016/s0016-7037(02)00926-2

Masson-Delmotte, V., Schulz, M., Abe-Ouchi, A., Beer, J., Ganopolski, A., González Rouco, J. F., et al. (2013). Information from paleoclimate archives. In Climate change 2013: The physical science basis. Contribution of working group I to the fifth assessment report of the intergovernmental panel on climate change. Cambridge, United Kingdom: Cambridge University Press.

Mcculloch, M. T., Gagan, M. K., Mortimer, G. E., Chivas, A. R., & Isdale, P. J. (1994). A high-resolution Sr/Ca and δ18O coral record from the Great Barrier Reef, Australia, and the 1982–1983 El Niño. *Geochimica et Cosmochimica Acta*, *58*(12), 2747–2754. https://doi.org/10.1016/0016-7037(94)90142-2

McGregor, H. V., Fischer, M. J., Gagan, M. K., Fink, D., Phipps, S. J., Wong, H., & Woodroffe, C. D. (2013). A weak El Niño/Southern Oscillation with delayed seasonal growth around 4,300 years ago. *Nature Geoscience*, *6*(11), 949–953. https://doi.org/10.1038/ngeo1936

Mitsuguchi, T., Dang, P. X., Kitagawa, H., Uchida, T., & Shibata, Y. (2008). Coral Sr/Ca and Mg/Ca records in Con Dao Island off the Mekong Delta: Assessment of their potential for monitoring ENSO and East Asian monsoon. *Global and Planetary Change*, *63*, 341–352. https://doi.org/10.1016/j.gloplacha.2008.08.002

Moy, C. M., Seltzer, G. O., Rodbell, D. T., & Anderson, D. M. (2002). Variability of EI Niño/Southern Oscillation activity at millennial timescales during the Holocene epoch. *Nature*, *420*(6912), 162–165. https://doi.org/10.1038/nature01194

Nurhati, I. S., Cobb, K. M., & Di Lorenzo, E. (2011). Decadal-scale SST and salinity variations in the central tropical Pacific: Signatures of natural and anthropogenic climate change. *Journal of Climate*, *24*(13), 3294–3308. https://doi.org/10.1175/2011jcli3852.1

Okai, T., Suzuki, A., Kawahata, H., Terashima, S., & Imai, N. (2002). Preparation of a new geological survey of Japan geochemical reference material: Coral JCp-1. *Geostandards Newsletter*, *26*(1), 95–99. https://doi.org/10.1111/j.1751-908x.2002.tb00627.x

Rayner, N. A., Parker, D. E., Horton, E. B., Folland, C. K., Alexander, L. V., Rowell, D. P., et al. (2003). Global analyses of sea surface temperature, sea ice, and night marine air temperature since the late nineteenth century. *Journal of Geophysical Research*, *108*(14). https://doi.org/10.1029/2002jd002670

Rein, B., Luckge, A., Reinhardt, L., Sirocko, F., Wolf, A., & Dullo, W. C. (2005). El Niño variability off Peru during the last 20,000 years. *Paleoceanography*, *20*(4), PA4003. https://doi.org/10.1029/2004pa001099

Reuter, J., Stott, L., Khider, D., Sinha, A., Cheng, H., & Edwards, R. L. (2009). A new perspective on the hydroclimate variability in northern south America during the Little Ice Age. *Geophysical Research Letters*, *36*, L21706. https://doi.org/10.1029/2009gl041051

Reynolds, R. W., Rayner, N. A., Smith, T. M., Stokes, D. C., & Wang, W. (2002). An improved in situ and satellite SST analysis for climate. *Journal of Climate*, *15*(13), 1609–1625. https://doi.org/10.1175/1520-0442(2002)015<1609:aiisas>2.0.co;2

Rustic, G. T., Koutavas, A., Marchitto, T. M., & Linsley, B. K. (2015). Dynamical excitation of the tropical Pacific Ocean and ENSO variability by Little Ice Age cooling. *Science*, *350*(6267), 1537–1541. https://doi.org/10.1126/science.aac9937

Sadekov, A. Y., Ganeshram, R., Pichevin, L., Berdin, R., McClymont, E., Elderfield, H., & Tudhope, A. W. (2013). Palaeoclimate reconstructions reveal a strong link between El Niño-Southern Oscillation and Tropical Pacific mean state. *Nature Communications*, *4*(1). https://doi.org/10.1038/ncomms3692

Salvatteci, R., Gutiérrez, D., Field, D., Sifeddine, A., Ortlieb, L., Bouloubassi, I., et al. (2013). The response of the Peruvian Upwelling Ecosystem to centennial-scale global change during the last two millennia. *Climate of the Past*, *9*(5), 5479–5519.

Sarachik, E. S., & Cane, M. A. (2010). *The El Niño-southern oscillation phenomenon* (pp. 336–384). Cambridge, United Kingdom: Cambridge University Press.

Sayani, H. R., Cobb, K. M., DeLong, K., Hitt, N. T., & Druffel, E. R. M. (2019). Inter-colony $\delta^{18}$O and Sr/Ca variability among Porites spp. corals at Palmyra Atoll: Toward more robust coral-based estimates of climate. *Geochemistry, Geophysics, Geosystems*, *20*(11), 5270–5284. https://doi.org/10.1029/2019GC008420

Schmidt, G. A. (2010). Enhancing the relevance of palaeoclimate model/data comparisons for assessments of future climate change. *Journal of Quaternary Science*, *25*, 79–87. https://doi.org/10.1002/jqs.1314

Schrag, D. P. (1999). Rapid analysis of high-precision Sr/Ca ratios in corals and other marine carbonated. *Paleoceanography*, *14*(2), 97–102. https://doi.org/10.1029/1998pa900025

Seager, R., Burgman, R., Kushnir, Y., Clement, A., Cook, E., Naik, N., et al. (2008). Tropical Pacific forcing of North American Medieval megadroughts: Testing the concept with an atmospheric model forced by coral-reconstructed SST. *Journal of Climate*, *21*(23), 6175–6190. https://doi.org/10.1175/2008jcli2170.1

Smith, S. V., Buddemeier, R. W., Redalje, R. C., & Houck, J. E. (1979). Strontium-Calcium thermometry in coral skeletons. *Science*, *204*(4391), 404–407. https://doi.org/10.1126/science.204.4391.404

Solow, A. R., & Huppert, A. (2004). A potential bias in coral reconstruction of sea surface temperature. *Geophysical Research Letters*, *31*(6), L06308. https://doi.org/10.1029/2003gl019349

Song, S., Peng, Z., Zhou, W., Liu, W., Liu, Y., & Chen, T. (2012). Variation of the winter monsoon in South China Sea over the past 183 years: Evidence from oxygen isotopes in coral. *Global and Planetary Change*, *98*(99), 131–138. https://doi.org/10.1016/j.gloplacha.2012.08.013

Steinhilber, F., Beer, J., & Frhlich, C. (2009). Total solar irradiance during the Holocene. *Geophysical Research Letters*, *36*(19). https://doi.org/10.1029/2009gl040142

Su, R., Sun, D., Chen, H., Chen, X., & Li, Z. (2010). Evolution of Asian monsoon variability revealed by oxygen isotopic record of middle Holocene massive coral in the northern South China Sea. *Quaternary International*, *213*(1–2), 56–68. https://doi.org/10.1016/j.quaint.2009.04.006

Sun, D., Gagan, M. K., Cheng, H., Gagan, H. S., Dykoski, C. A., Edwards, R. L., & Su, R. (2005). Seasonal and interannual variability of the Mid-Holocene East Asian monsoon in coral $\delta^{18}$O records from the South China Sea. *Earth and Planetary Science Letters*, *237*(1–2), 69–84. https://doi.org/10.1016/j.epsl.2005.06.022

Tan, L., Shen, C., Löwemark, L., Chawchai, S., Edwards, R. L., Cai, Y., et al. (2019). Rainfall variations in central Indo-Pacific over the past 2,700 y. In *Proceedings of the national academy of sciences* (*116*(35), pp. 17201–17206). https://doi.org/10.1073/pnas.1903167116

Tierney, J. E., Abram, N. J., Anchukaitis, K. J., Evans, M. N., Giry, C., Kilbourne, K. H., et al. (2015). Tropical sea surface temperatures for the past four centuries reconstructed from coral archives. *Paleoceanography*, *30*, 226–252. https://doi.org/10.1002/2014pa002717

Tierney, J. E., Oppo, D. W., Rosenthal, Y., Russell, J. M., & Linsley, B. K. (2010). Coordinated hydrological regimes in the Indo-Pacific region during the past two millennia. *Paleoceanography*, *25*(1), PA1102. https://doi.org/10.1029/2009pa001871

Timmermann, A., An, S., Kug, J., Jin, F., Cai, W., Capotondi, A., et al. (2018). El Niño–Southern Oscillation complexity. *Nature*, *559*(7715), 535–545.

Torrence, C., & Compo, G. P. (1998). A practical guide to wavelet analysis. *Bulletin of the American Meteorological Society*, *79*, 61–78. https://doi.org/10.1175/1520-0477(1998)079<0061:apgtwa>2.0.co;2

Toth, L. T., Aronson, R. B., Cobb, K. M., Cheng, H., Edwards, R. L., Grothe, P. R., & Sayani, H. R. (2015). Climatic and biotic thresholds of coral-reef shutdown. *Nature Climate Change*, *5*(4), 369–374. https://doi.org/10.1038/nclimate2541

Trenberth, K. E. (1984). Signal versus noise in the Southern Oscillation. *Monthly Weather Review*, *112*(2), 326–332. https://doi.org/10.1175/1520-0493(1984)112<0326:svnits>2.0.co;2

Trenberth, K. E. (1997). The definition of El Niño. *Bulletin of the American Meteorological Society*, *78*(12), 2771–2777. https://doi.org/10.1175/1520-0477(1997)078<2771:tdoeno>2.0.co;2

Tudhope, A. W., Chilcott, C. P., McCulloch, M. T., Cook, E. R., Chappell, J., Ellam, R. M., et al. (2001). Variability in the El Niño-Southern Oscillation through a glacial-interglacial cycle. *Science*, *291*(5508), 1511–1517. https://doi.org/10.1126/science.1057969

Wang, B., Wu, R., & Fu, X. (2000). Pacific–East Asian teleconnection: How does ENSO affect East Asian climate? *Journal of Climate*, *13*(9), 1517–1536. https://doi.org/10.1175/1520-0442(2000)013<1517:peathd>2.0.co;2

Wang, C., Wang, W., Wang, D., & Wang, Q. (2006). Interannual variability of the South China Sea associated with El Niño. *Journal of Geophysical Research*, *111*, C03023. https://doi.org/10.1029/2005jc003333

Wang, C. Z., & Fiedler, P. C. (2006). ENSO variability and the eastern tropical pacific: A review. *Progress in Oceanography*, *69*(2–4), 239–266. https://doi.org/10.1016/j.pocean.2006.03.004

Wang, D., Liu, Q., Liu, Y., & Shi, P. (2004). Connection between interannual variability of the western Pacific and eastern Indian Oceans in the 1997~1998 El Niño event. *Progress in Natural Science*, *14*(5), 423–429. https://doi.org/10.1080/10020070412331343721

Wang, X., Deng, W., Liu, X., Wei, G., Chen, X., Zhao, J., et al. (2018). Super instrumental El Niño events recorded by a *Porites* coral from the South China Sea. *Coral Reefs*, *37*(1), 295–308. https://doi.org/10.1007/s00338-018-1658-1

Wei, G. J., Deng, W. F., Yu, K. F., Li, X. H., Sun, W. D., & Zhao, J. X. (2007). Sea surface temperature records in the northern South China Sea from mid-Holocene coral Sr/Ca ratios. *Paleoceanography*, *22*(3), PA3206. https://doi.org/10.1029/2006pa001270

Wilson, R., Cook, E., D'Arrigo, R., Riedwyl, N., Evans, M. N., Tudhope, A., & Allan, R. (2010). Reconstructing ENSO: The influence of method, proxy data, climate forcing and teleconnections. *Journal of Quaternary Science*, *25*(1), 62–78. https://doi.org/10.1002/jqs.1297

Wittenberg, A. T. (2009). Are historical records sufficient to constrain ENSO simulations? *Geophysical Research Letters*, *36*, L12702. https://doi.org/10.1029/2009gl038710

Yan, H., Liu, C., Zhang, W., Li, M., Zheng, X., Wei, G., et al. (2017). ENSO variability around 2000 years ago recorded by *Tridacna gigas* $\delta^{18}$O from the South China Sea. *Quaternary International*, *452*, 148–154. https://doi.org/10.1016/j.quaint.2016.05.011

Yan, H., Soon, W., & Wang, Y. (2015). A composite sea surface temperature record of the northern South China Sea for the past 2500 years: A unique look into seasonality and seasonal climate changes during warm and cold periods. *Earth-Science Reviews*, *141*, 122–135. https://doi.org/10.1016/j.earscirev.2014.12.003

Yan, H., Sun, L., Liu, X., & Qiu, S. (2010). Relationship between ENSO events and regional climate anomalies around the Xisha Islands during the last 50 years. *Journal of Tropical Oceanography*, *29*(05), 29–35.

Yan, H., Sun, L., Wang, Y., Huang, W., Qiu, S., & Yang, C. (2011). A record of the Southern Oscillation Index for the past 2,000 years from precipitation proxies. *Nature Geoscience*, *4*(9), 611–614. https://doi.org/10.1038/ngeo1231

Yu, K. F. (2012). Coral reefs in the South China Sea: Their response to and records on past environmental changes. *Science China Earth Sciences*, *42*(8), 1160–1172. https://doi.org/10.1007/s11430-012-4449-5

Yu, K. F., Zhao, J., Shi, Q., Chen, T., Wang, P., & Collerson, K. D., & Liu, T. (2006). U-series dating of dead *Porites* corals in the South China sea: Evidence for episodic coral mortality over the past two centuries. *Quaternary Geochronology*, *1*(2), 129–141. https://doi.org/10.1016/j.quageo.2006.06.005

Yu, K. F., Zhao, J. X., Liu, T. S., Wei, G. J., Wang, P. X., & Collerson, K. D. (2004). High-frequency winter cooling and reef coral mortality during the Holocene climatic optimum. *Earth and Planetary Letters*, *224*(1–2), 143–155. https://doi.org/10.1016/j.epsl.2004.04.036

Yu, K. F., Zhao, J. X., Shi, Q., & Price, G. J. (2012). Recent massive coral mortality events in the South China Sea: Was global warming and ENSO variability responsible? *Chemical Geology*, *320–321*, 54–65. https://doi.org/10.1016/j.chemgeo.2012.05.028

Yu, K. F., Zhao, J. X., Wei, G. J., Cheng, X. R., & Wang, P. X. (2005). Mid–late Holocene monsoon climate retrieved from seasonal Sr/Ca and δ¹⁸O records of *Porites lutea* corals at Leizhou Peninsula, northern coast of South China Sea. *Global and Planetary Change*, *47*(2–4), 301–316. https://doi.org/10.1016/j.gloplacha.2004.10.018

Zhu, Q., & Xie, L. (1988). 1986–87 northern winter Asia/Australia circulation anomalies with their relation to the western Pacific SST. *Journal of Tropical Meteorology*, *4*(3), 254–262.(in Chinese with English abstract).